This is a repository copy of *Sub-clinical assessment of atopic dermatitis severity using angiographic optical coherence tomography*.

White Rose Research Online URL for this paper:
http://eprints.whiterose.ac.uk/129762/

Version: Published Version

Article:

Sub-clinical assessment of atopic dermatitis severity using angiographic optical coherence tomography

ROBERT A. BYERS,[1,*] RAMAN MAITI,[2] SIMON G. DANBY,[3] ELAINE J. PANG,[3] BETHANY MITCHELL,[3] MATT J. CARRÉ,[2] ROGER LEWIS,[2] MICHAEL J. CORK,[3] AND STEPHEN J. MATCHER[1]

[1]*Department of Electronic and Electrical Engineering, University of Sheffield, Sheffield, UK*
[2]*Department of Mechanical Engineering, University of Sheffield, Sheffield, UK*
[3]*Sheffield Dermatology Research, Department of Infection, Immunity & Cardiovascular Disease, The Royal Hallamshire Hospital, University of Sheffield, Sheffield, UK*
*rabyers1@sheffield.ac.uk

Abstract: Measurement of sub-clinical atopic dermatitis (AD) is important for determining how long therapies should be continued after clinical clearance of visible AD lesions. An important biomarker of sub-clinical AD is epidermal hypertrophy, the structural measures of which often make optical coherence tomography (OCT) challenging due to the lack of a clearly delineated dermal-epidermal junction in AD patients. Alternatively, angiographic OCT measurements of vascular depth and morphology may represent a robust biomarker for quantifying the severity of clinical and sub-clinical AD. To investigate this, angiographic data sets were acquired from 32 patients with a range of AD severities. Deeper vascular layers within skin were found to correlate with increasing clinical severity. Furthermore, for AD patients exhibiting no clinical symptoms, the superficial plexus depth was found to be significantly deeper than healthy patients at both the elbow (p = 0.04) and knee (p<0.001), suggesting that sub-clinical changes in severity can be detected. Furthermore, the morphology of vessels appeared altered in patients with severe AD, with significantly different vessel diameter, length, density and fractal dimension. These metrics provide valuable insight into the sub-clinical severity of the condition, allowing the effects of treatments to be monitored past the point of clinical remission.

References and links

1. T. E. Shaw, G. P. Currie, C. W. Koudelka, and E. L. Simpson, "Eczema Prevalence in the United States: Data from the 2003 National Survey of Children's Health," J. Invest. Dermatol. **131**(1), 67–73 (2011).
2. J. A. Odhiambo, H. C. Williams, T. O. Clayton, C. F. Robertson, and M. I. Asher, "Global variations in prevalence of eczema symptoms in children from ISAAC Phase Three," J. Allergy Clin. Immunol. **124**(6), 1251 (2009).
3. J. I. Silverberg and J. M. Hanifin, "Adult eczema prevalence and associations with asthma and other health and demographic factors: a US population-based study," J. Allergy Clin. Immunol. **132**(5), 1132–1138 (2013).
4. S. T. Holgate, "The epidemic of allergy and asthma," Nature **402**(6760), B2–B4 (1999).
5. T. Bieber, "Atopic Dermatitis," N. Engl. J. Med. **358**(14), 1483–1494 (2008).
6. M. J. Cork, S. G. Danby, Y. Vasilopoulos, J. Hadgraft, M. E. Lane, M. Moustafa, R. H. Guy, A. L. Macgowan, R. Tazi-Ahnini, and S. J. Ward, "Epidermal Barrier Dysfunction in Atopic Dermatitis," J. Invest. Dermatol. **129**(8), 1892–1908 (2009).
7. European Task Force on Atopic Dermatitis, "Severity scoring of atopic dermatitis: the SCORAD index," Dermatology (Basel) **186**(1), 23–31 (1993).
8. J. M. Hanifin, M. Thurston, M. Omoto, R. Cherill, S. J. Tofte, and M. Graeber, "The eczema area and severity index (EASI): assessment of reliability in atopic dermatitis," Exp. Dermatol. **10**(1), 11–18 (2001).
9. T. S. Tang, T. Bieber, and H. C. Williams, "Are the concepts of induction of remission and treatment of subclinical inflammation in atopic dermatitis clinically useful?" J. Allergy Clin. Immunol. **133**(6), 1615–25.e1 (2014).

10. S. Seidenari and G. Giusti, "Objective assessment of the skin of children affected by atopic dermatitis: a study of pH, capacitance and TEWL in eczematous and clinically uninvolved skin," Acta Derm. Venereol. **75**(6), 429–433 (1995).

11. J. Gupta, E. Grube, M. B. Ericksen, M. D. Stevenson, A. W. Lucky, A. P. Sheth, A. H. Assa'ad, and G. K. Khurana Hershey, "Intrinsically defective skin barrier function in children with atopic dermatitis correlates with disease severity," J. Allergy Clin. Immunol. **121**(3), 725–730.e2 (2008).

12. M. Suárez-Fariñas, S. J. Tintle, A. Shemer, A. Chiricozzi, K. Nograles, I. Cardinale, S. Duan, A. M. Bowcock, J. G. Krueger, and E. Guttman-Yassky, "Nonlesional atopic dermatitis skin is characterized by broad terminal differentiation defects and variable immune abnormalities," J. Allergy Clin. Immunol. **127**(4), 954–64.e1, 4 (2011).

13. J. Welzel, M. Bruhns, and H. H. Wolff, "Optical coherence tomography in contact dermatitis and psoriasis," Arch. Dermatol. Res. **295**(2), 50–55 (2003).

14. J. Delacruz, J. Weissman, and K. Gossage, "Automated measurement of epidermal thickness from optical coherence tomography images using line region growing," in Proc. SPIE 7548. Photonic Therapeutics and Diagnostics **VI**, 75480E (2010).

15. R. Maiti, L. C. Gerhardt, Z. S. Lee, R. A. Byers, D. Woods, J. A. Sanz-Herrera, S. E. Franklin, R. Lewis, S. J. Matcher, and M. J. Carré, "In vivo measurement of skin surface strain and sub-surface layer deformation induced by natural tissue stretching," J. Mech. Behav. Biomed. Mater. **62**, 556–569 (2016).

16. M. Cossmann and J. Welzel, "Evaluation of the atrophogenic potential of different glucocorticoids using optical coherence tomography, 20-MHz ultrasound and profilometry; a double-blind, placebo-controlled trial," Br. J. Dermatol. **155**(4), 700–706 (2006).

17. J. Boadi, Z. Lu, S. Danby, M. Cork, and S. J. Matcher, "Optical coherence tomography demonstrates differential epidermal thinning of human forearm volar skin after 2 weeks application of a topical corticosteroid vs a non-steroidal anti-inflammatory alternative," in Proc. SPIE 8565. Photonic Therapeutics and Diagnostics **IX**, 85650C (2013).

18. G. Josse, C. Rouvrais, A. Mas, M. Haftek, A. Delalleau, Y. Ferraq, F. Ossant, J. George, J. M. Lagarde, and A. M. Schmitt, "A multitechnique evaluation of topical corticosteroid treatment," Skin Res. Technol. **15**(1), 35–39 (2009).

19. L. Kolbe, A. M. Kligman, V. Schreiner, and T. Stoudemayer, "Corticosteroid-induced atrophy and barrier impairment measured by non-invasive methods in human skin," Skin Res. Technol. **7**(2), 73–77 (2001).

20. A. Mariampillai, B. A. Standish, E. H. Moriyama, M. Khurana, N. R. Munce, M. K. Leung, J. Jiang, A. Cable, B. C. Wilson, I. A. Vitkin, and V. X. Yang, "Speckle variance detection of microvasculature using swept-source optical coherence tomography," Opt. Lett. **33**(13), 1530–1532 (2008).

21. R. A. Byers, G. Tozer, N. J. Brown, and S. J. Matcher, "High-resolution label-free vascular imaging using a commercial, clinically approved dermatological OCT scanner," in Proc. SPIE 9689. Photonic Therapeutics and Diagnostics **XII**, 96890M (2016).

22. M. Ulrich, L. Themstrup, N. de Carvalho, M. Manfredi, C. Grana, S. Ciardo, R. Kästle, J. Holmes, R. Whitehead, G. B. E. Jemec, G. Pellacani, and J. Welzel, "Dynamic Optical Coherence Tomography in Dermatology," Dermatology (Basel) **232**(3), 298–311 (2016).

23. E. Y. Lam and J. W. Goodman, "A mathematical analysis of the DCT coefficient distributions for images," IEEE Trans. Image Process. **9**(10), 1661–1666 (2000).

24. M. Steinhoff, A. Steinhoff, B. Homey, T. A. Luger, and S. W. Schneider, "Role of vasculature in atopic dermatitis," J. Allergy Clin. Immunol. **118**(1), 190–197 (2006).

25. S. S. Wong, C. Edwards, and R. Marks, "A study of white dermographism in atopic dermatitis," J. Dermatol. Sci. **11**(2), 148–153 (1996).

26. R. A. Byers, M. Fisher, N. J. Brown, G. M. Tozer, and S. J. Matcher, "Vascular patterning of subcutaneous mouse fibrosarcomas expressing individual VEGF isoforms can be differentiated using angiographic optical coherence tomography," Biomed. Opt. Express **8**(10), 4551–4567 (2017).

27. M. Guizar-Sicairos, S. T. Thurman, and J. R. Fienup, "Efficient subpixel image registration algorithms," Opt. Lett. **33**(2), 156–158 (2008).

28. A. F. Frangi, W. J. Niessen, K. L. Vincken, and M. A. Viergever, "Multiscale vessel enhancement filtering," in *International Conference on Medical Image Computing and Computer-Assisted Intervention* **1496**, 130–137 (1998).

29. N. Otsu, "A Threshold Selection Method from Gray-Level Histograms," IEEE Trans. Syst. Man Cybern. **9**(1), 62–66 (1979).

30. P. Soille, "Geodesic Transformations," in *Morphological Image Analysis* (Springer Berlin Heidelberg, 2004), pp. 183–218.

31. K. Jurczyszyn, B. J. Osiecka, and P. Ziółkowski, "The Use of Fractal Dimension Analysis in Estimation of Blood Vessels Shape in Transplantable Mammary Adenocarcinoma in Wistar Rats after Photodynamic Therapy Combined with Cysteine Protease Inhibitors," Comput. Math. Methods Med. **2012**, 1–6 (2012).

32. R. A. Byers, R. Maiti, S. G. Danby, E. J. Pang, B. Mitchell, M. J. Carré, R. Lewis, M. J. Cork, and S. J. Matcher, "Characterizing the microcirculation of atopic dermatitis using angiographic optical coherence tomography," Proc. SPIE **10037**, Photonics in Dermatology and Plastic Surgery, 100370V (2017).

33. B. J. Vakoc, R. M. Lanning, J. A. Tyrrell, T. P. Padera, L. A. Bartlett, T. Stylianopoulos, L. L. Munn, G. J. Tearney, D. Fukumura, R. K. Jain, and B. E. Bouma, "Three-dimensional microscopy of the tumor

microenvironment in vivo using optical frequency domain imaging," Nat. Med. **15**(10), 1219–1223 (2009).

34. G. M. Drzewiecki and J. K.-J. Li, *Analysis and Assessment of Cardiovascular Function* (Springer, 1998).

35. G. Abignano, S. Z. Aydin, C. Castillo-Gallego, V. Liakouli, D. Woods, A. Meekings, R. J. Wakefield, D. G. McGonagle, P. Emery, and F. Del Galdo, "Virtual skin biopsy by optical coherence tomography: the first quantitative imaging biomarker for scleroderma," Ann. Rheum. Dis. **72**(11), 1845–1851 (2013).

36. M. C. Mihm, Jr., N. A. Soter, H. F. Dvorak, and K. F. Austen, "The Structure Of Normal Skin And The Morphology Of Atopic Eczema," J. Invest. Dermatol. **67**(3), 305–312 (1976).

37. L. Barnes, G. Kaya, and V. Rollason, "Topical Corticosteroid-Induced Skin Atrophy: A Comprehensive Review," Drug Saf. **38**(5), 493–509 (2015).

38. G. Varricchi, F. Granata, S. Loffredo, A. Genovese, and G. Marone, "Angiogenesis and lymphangiogenesis in inflammatory skin disorders," J. Am. Acad. Dermatol. **73**(1), 144–153 (2015).

39. D. A. Groneberg, C. Bester, A. Grützkau, F. Serowka, A. Fischer, B. M. Henz, and P. Welker, "Mast cells and vasculature in atopic dermatitis-potential stimulus of neoangiogenesis," Allergy **60**(1), 90–97 (2005).

40. C. Schuster, J. Smolle, W. Aberer, and B. Kränke, "Vascular pattern of the palms-A clinical feature of atopic skin diathesis," Allergy **61**(12), 1392–1396 (2006).

41. R. Aschoff, U. Schwanebeck, M. Bräutigam, and M. Meurer, "Skin physiological parameters confirm the therapeutic efficacy of pimecrolimus cream 1% in patients with mild-to-moderate atopic dermatitis," Exp. Dermatol. **18**(1), 24–29 (2009).

42. B. Zabihian, J. Weingast, M. Liu, E. Zhang, P. Beard, H. Pehamberger, W. Drexler, and B. Hermann, "In vivo dual-modality photoacoustic and optical coherence tomography imaging of human dermatological pathologies," Biomed. Opt. Express **6**(9), 3163–3178 (2015).

43. R. Huggenberger and M. Detmar, "The cutaneous vascular system in chronic skin inflammation," J. Investig. Dermatol. Symp. Proc. **15**(1), 24–32 (2011).

44. Z. Samochocki, J. Bogaczewicz, A. Sysa-Jędrzejowska, D. P. McCauliffe, E. Kontny, and A. Wozniacka, "Expression of vascular endothelial growth factor and other cytokines in atopic dermatitis, and correlation with clinical features," Int. J. Dermatol. **55**(3), e141–e146 (2016).

45. Y. Zhang, H. Matsuo, and E. Morita, "Increased production of vascular endothelial growth factor in the lesions of atopic dermatitis," Arch. Dermatol. Res. **297**(9), 425–429 (2006).

46. M. Detmar, "The role of VEGF and thrombospondins in skin angiogenesis," J. Dermatol. Sci. **24**(1), S78–S84 (2000).

47. D. Mancardi, G. Varetto, E. Bucci, F. Maniero, and C. Guiot, "Fractal parameters and vascular networks: facts & artifacts," Theor. Biol. Med. Model. **5**(1), 12 (2008).

1. Introduction

Atopic dermatitis (AD – synonym atopic eczema) is a chronic, inflammatory disorder of the skin which has a profound effect on quality of life. The prevalence of the condition within the US is estimated to be approximately 10.7% for child AD [1] (Global – 7.3% [2]) and 10.2% for adult AD [3], and is generally increasing within both the developed and developing world [2,4]. Symptoms include dry, itchy, erythematous skin, which exhibit abnormalities such as increased trans-epidermal water loss (TEWL) [5]. These symptoms arise due to complex interactions between many different genes and environmental factors, which lead to a defective epidermal barrier and Th 2 driven inflammation [6]. Clinical assessment of the extent and severity of AD is typically performed using external grading systems such as the severity scoring of AD [7] (SCORAD) or the eczema area and severity index [8] (EASI) which look for specific signs and coverage of the condition. These externally visible signs include erythema, edema, papulation, excoriation, lichenification and oozing [8]. There is however substantial evidence that unaffected, lesion-free skin sites of AD patients can remain abnormal, even following remission of the condition [9]. Such "subclinical" abnormalities include significant differences in TEWL, pH and capacitance between healthy and unaffected skin [10,11] as well as structural abnormalities such as epidermal thickening [9,12]. Indeed it appears clear that externally healthy looking skin of previously diagnosed AD patients is likely to contain hidden abnormalities beneath the skin surface [12]. Identification of these subclinical factors could facilitate improved treatments which aim to monitor and suppress progression of the disorder past the point of clinical remission [9].

Optical Coherence Tomography (OCT) is an established non-invasive medical-imaging technique which utilizes near-infrared light to capture a reflectance profile of the sub-surface layers within skin. Previous studies have utilized the high axial resolution (~5-10μm) of OCT to delineate the dermal-epidermal junction (DEJ) within skin, allowing for automated

measurements of epidermal thickness [13–15]. In the context of AD, measurements of epidermal atrophy (thinning) following corticosteroid treatment have been well documented using both OCT [16–18] and other non-invasive modalities [18,19]. In contrast, epidermal thickening, associated with skin inflammation [12], is more challenging to accurately quantify using simple structural OCT, owing to a reduction in contrast between the epidermal and dermal layers of the skin as the epidermis thickens and the dermal papillae extend upwards (Sec. 3.2). To avoid subjective and time-consuming manual measurements of epidermal thickness, an alternative method of quantifying the degree of thickening could be to measure the depth of vascular layers of the skin. Firstly, the superficial plexus which lies horizontally in the upper papillary dermis could be considered a lower boundary for the true DEJ location. Secondly, the tips of the capillary loops which extend vertically into each of the dermal papillae represent the thinnest points of the epidermis and could be considered an upper boundary for the DEJ location (Fig. 1). The depths of these vessel layers are likely to be influenced by inflammation, as a thickening epidermis will push the superficial plexus deeper into the tissue.
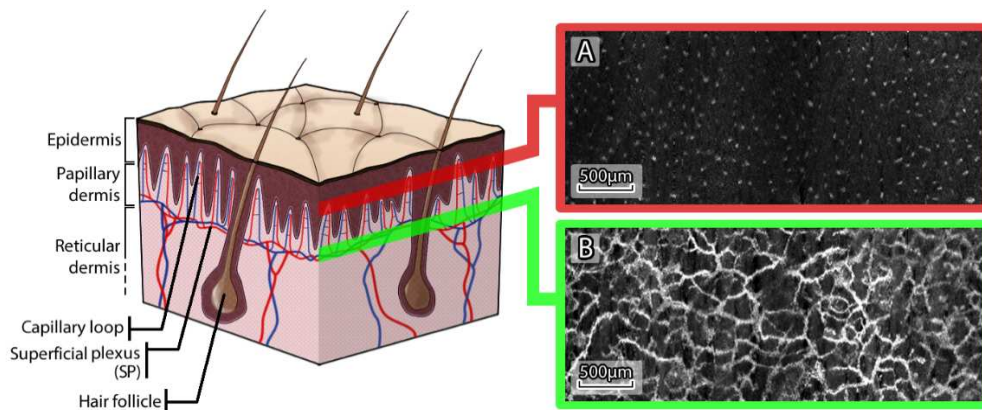

Fig. 1. The structure of skin affected by epidermal thickening (Sebaceous glands and sweat ducts omitted for clarity). Vertical arteries and capillaries rise from the deep plexus and form a horizontal network termed the superficial plexus (SP). From this, capillary loops consisting of both rising arterioles and falling venules form hairpin like structures in the dermal papillae. A) An en-face angiographic svOCT image captured at a depth corresponding to the tips of the capillary loops, visible as small dots in the en-face perspective. B) An en-face angiographic svOCT image captured at a depth corresponding to the SP. Large interconnected vessels are visible. The depth of these layers may provide a direct measure of the tissue inflammation.

Recently developed processing methods have enabled the extraction of three-dimensional angiographic data from oversampled structural OCT data sets [20,21], which has enabled further study of numerous dermatological conditions [22]. One such method, termed speckle-variance OCT (svOCT) identifies the presence of fluid flow by considering the temporal evolution of intensity (speckle) within each pixel of a volume. Pixels in a solid region of tissue exhibit intensities which can be characterized by a Gaussian distribution, due to static coherent speckle and random acquisition noise. Comparatively, pixels in a fluid region of tissue will exhibit intensities in a Rayleigh distribution, as a combination of both acquisition noise and moving speckle [23]. This gives rise to contrast between solid and fluid regions of the skin.

The aims of this study are two-fold: firstly, we aim to develop and validate angiographic OCT for automated measurements of epidermal thickness within skin affected with a range of AD severities. Secondly, we aim to investigate whether subclinical morphological differences within the microcirculation of AD patients correlate with the severity of the condition.

2. Materials and methods

2.1 Participants

A total of 32 volunteers were recruited for this study. Both male and female volunteers aged 18-60 with Fitzpatrick skin type I-III (Mexameter melanin reading of <350) were considered on a first-come first served basis. Exclusion criteria included pregnancy, folliculitis, acne, suntan, hyperpigmentation, multiple nevi, tattoos, blemishes or dense body hair in the test areas. Cosmetic products were also restricted prior to the study initiation. Of the 32 participants; 5 were healthy, having no prior history of any chronic skin condition (Including AD). The remaining 27 participants had currently active AD (As defined by the UK working party diagnostic criteria) at a range of severities, as well as having no history of any other chronic skin conditions. Informed consent was obtained from each participant prior to imaging. The National Research Ethics Service (NRES) Committee East Midlands–Derby, formally known as Trent Multicentre Research Ethics Committee (MREC), approved the study, under the project reference 04/MREC/70.

2.2 Imaging protocol

All imaging for this study was performed using a multi-beam OCT system (Vivosight, Michelson Diagnostics Ltd, Orpington, Kent, UK) running at 20 kHz line acquisition rate. This system utilizes a swept-source 1305nm Axsun laser with a bandwidth of 147nm, allowing visualization of structures to a depth of ~1mm in skin. Four imaging sites which commonly exhibit AD symptoms were chosen for the study, these being the left and right cubital fossa (crook of the elbow) as well as the left and right popliteal fossa (crook of the knee).
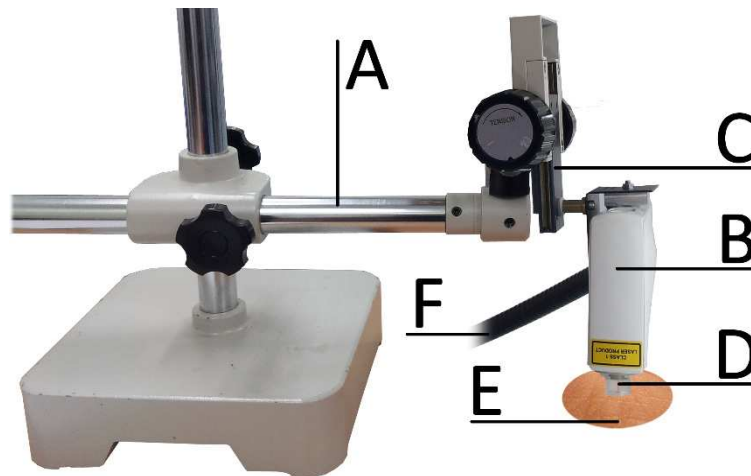

Fig. 2. The OCT imaging set-up used for this study. A mechanical clamp (A) was used to fix the Vivosight imaging probe (B) into place above the region of interest. The vertical stage of the clamp (C) was then lowered such that the plastic cap (D) gently touched the surface of the skin (E). This plastic cap reduced any lateral (sliding) motion between the probe and the skin. Data was then transferred to the optical processing unit of the OCT system through a cable (F).

Prior to imaging, each participant was asked to wait 20 minutes in the study room with the skin of the test sites exposed, this process aimed to acclimatize each of the test sites such that any homeostatic variance was minimized. Following this, each skin site of the participant was assessed independently by two different graders to establish severity scores based on dryness, erythema, edema/papulation, excoriation and lichenification, assigning a number between 0 and 3 for each. A local EASI score for each specific skin site was defined as the sum of each of these severity scores, averaged between the two assessors. A global (full-body) EASI score

was calculated for each participant through a similar scoring and area coverage assessment at the head/neck, upper limbs, trunk and lower limb regions following previously described weighting and methodology [8]. The handheld probe of the OCT system was then positioned for imaging using a mechanical clamp, such that any movement artifacts originating from the operator were eliminated. A plastic cap bridged the gap between the OCT probe and the skin, which was deemed necessary to reduce any lateral sliding of the skin surface during imaging. The OCT imaging set-up is illustrated in Fig. 2. Given that the imaging protocol involves physical contact with the skin surface, one might expect some degree of vasoconstriction through the white dermographism response which is common within AD affected skin [24]. White dermographism within AD is known to have a relatively long onset ($23 \pm 1.4s$) with comparatively short duration ($6 \pm 1s$) [25]. Thus, in order to reduce the influence of this effect on the resulting vascular data, a delay of approximately 30 seconds was added following the fixation of the imaging probe.

Imaging was then performed, with four-dimensional (x-y-z-time) structural OCT volumes being collected from each skin site in turn. All scans captured a volume of 4x4x2mm with 10 repeat B-scans being collected at each y-location such that a measure of variance could be calculated as per the svOCT methodology. The first 12 AD patient data sets were acquired with a 10μm A-scan spacing in the x-direction (fast scan) and a 20μm A-scan spacing in the y-direction (slow scan), with these scans taking approximately 50 seconds to acquire and save (40-frames/s). While the angiographic quality of these scans was sufficiently high for vessel depth measurement, the decision was made to increase the A-scan spacing in the y-direction to 10μm such that uniform spacing between scans was achieved, further increasing scan quality while doubling the required acquisition time. The remaining 20 data sets were acquired with this 10μm A-scan spacing (In both x and y) with each scan taking approximately 100 seconds to acquire and save. The increased resolution of these scans had no notable effect on the measurement of vascular layers (Sec. 2.4) but greatly enhanced the vascular morphology measurements (Sec. 2.3), thus quantification of vascular morphology was restricted only to data sets which were acquired with the higher resolution. The raw data was processed offline in MATLAB (R2014b – MathWorks) into an angiographic format following a previously described methodology [21,26]. Motion artefacts were suppressed by registering each of the repeat B-scans to the first B-scan captured at each location, using a sub-pixel accurate cross-correlation based algorithm to an accuracy of 100th of a pixel [27]. A combined wavelet-FFT filter was then utilized to effectively suppress any remaining motion artefacts with minimal degradation to the underlying vascular information [21,26]. This filter works by considering that a vertical line artefact has a high-frequency component in the horizontal (x) direction and a low frequency component in the vertical (y) direction. Vertical information within the volume is first extracted through wavelet decomposition, which high-pass filters the rows and low-pass filters the columns. The resulting image is then Fourier transformed, and frequency components along the x-axis are suppressed using a damping function. The image is then inverse Fourier transformed and repackaged together with its corresponding detail, horizontal and diagonal wavelet bands. Further details of this filter can be found in a previous publication [26].

2.3 Automatic quantification of vascular morphology

For both automatic quantification of microvessel morphology and plexus depth (Sec. 2.4) it was necessary to binarize the angiographic data such that vascular skeletons could be generated. Figure 3 shows the steps that were taken to skeletonize the data.
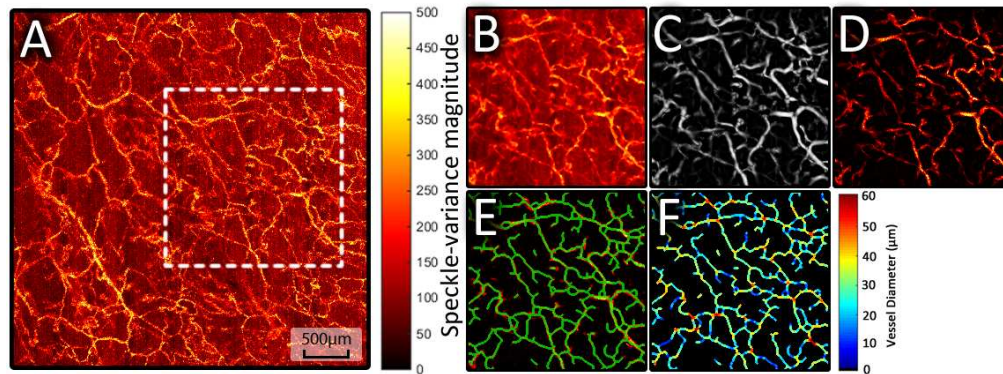
Fig. 3. Steps taken to skeletonize and quantify vascular parameters from angiographic data sets. A) *En-face* mean intensity projection captured from the popliteal fossa site of a healthy participant. White box shows the FOV used for B-G. B) Median filtering step. C) Multiscale Hessian filtering. D) Result of masking B with the "vesselness" data in C. E) Resulting skeleton (Green) overlaid on the masked data. F) Measured vessel diameter at each point along the vessel.

Firstly, an angiographic image was generated by performing mean-intensity-projections (MIP) over the depth range of interest (Fig. 3(A)), this image was median filtered to remove noise (Fig. 3(B)). The image was then processed with a Hessian filtering algorithm [28], which quantifies the "vesselness" of a pixel through consideration of the eigenvalues of the local Hessian matrix. To minimize artificial vessel dilation following Hessian filtering, a multi-scale approach was used. Compared to a single-scale approach, which uses gaussian kernels with a single value of σ in order to build the Hessian matrix, the multi-scale approach uses a range of σ values in order to consider a range of vessel scales. Here values of 1:10 were used for σ, corresponding to vessel scales of 10-100μm, with the strongest detection (maximum value) of each pixel across all vessel scales being recorded (Fig. 3(C)). The values of σ were selected empirically and offered reliable performance over the vessel scales observed here, with minimal vessel dilation being qualitatively visible. The filtered image was then used to compose a mask for the original data, preserving only areas of signal which were likely to be vascular derived (Fig. 3(D)). These filtering steps were deemed necessary due to the large magnitude of svOCT background noise, some of which is derived from movement of the participant during imaging. Following these steps, the image was binarized using an automatically determined threshold (Otsu's method [29]), with this binary image then being used to generate a vessel skeleton (Fig. 3(E)).

Four quantitative parameters were extracted using both the binarized data together with the vascular skeleton. Average vessel diameter (μm) was defined as double the average distance from the skeleton to the closest zero in the binarized image. Average vessel length (μm) was defined as the average length of skeleton segments between branching points in the skeleton, measured using a geodesic distance transform [30]. Vessel density (Vessels/mm^2) was calculated by dividing the total number of vessel segments in the image by the size of the area (16mm^2). Lastly, the fractal dimension of the skeleton network was calculated using the box-counting method [31], which outputs a value between 0 and 3, with higher values indicating a more irregular and tortuous network.

2.4 Automatic quantification of vascular depth

As discussed in Sec. 1, the capillary loop depth (CLD) and superficial plexus depth (SPD) within skin could potentially be used as a robust measure of acanthosis (epidermal hypertrophy). In our previous work, measurements of CLD and SPD were acquired qualitatively through visual observation of an *en-face* flythrough of the corresponding angiographic data [32]. Here, the skeletonization procedure outlined in Sec. 2.3 is used to

automate this step. Firstly, a pseudo-3D skeleton was generated over the entire visible depth range (0-1mm) by applying the skeletonization methodology to each z-depth in turn. With OCT angiography, forward scattering of photons by the red blood cells result in a shadowing artefact beneath detected vasculature [33]. This effect was utilized to improve the skeletonization further, as signal derived from the vasculature was present over a range of depths within the tissue, while noise-derived signal was inconsistent with respect to depth. A simple median filter of 3-pixel window size in the z-direction was used to remove skeleton points which were inconsistent with depth. The total number of independent skeleton segments was then calculated for each z-depth in the volume. In this context, an independent skeleton section was defined as a section of skeleton that was disconnected from other sections of the skeleton. As there is no vasculature present in the upper sections of the epidermis, there were no independent skeleton segments detected for superficial depths. Once the tips of capillary loops start entering the field-of-view (typically around 40-100μm in depth) the number of independent skeleton segments increased rapidly until reaching a local maximum. This maximum value represents the point at which the maximum number of unconnected capillary loops are visible, and is thus defined as the CLD. Typically at the CLD depth, between 200 and 500 independent skeleton sections were observed (corresponding to 13-31 capillaries per mm^2), this is in agreement with known measurements of the capillary density within skin, which typically range from 10 to 70 capillaries per mm^2 of skin [34]. Following the CLD, one might expect the number of independent skeleton segments to plateau as subsequent depths are simply following each loop along its axis. Instead, the value gradually reduces, suggesting that the vessel network almost immediately begins to interconnect. This is potentially a direct result of the ascending and descending limbs of each capillary loop spreading slightly apart with depth, as OCT lacks the resolution to clearly discriminate between each limb. The result is a dilation of the visible loops, with neighboring loops potentially merging together though not physically connected. At sufficient depth, the gradient of the curve of skeleton segment number vs depth reaches 0, suggesting that the network is fully connected; this point is defined as the SPD. The SPD depth was more challenging to automatically quantify, owing to an increase in noise and a lack of OCT signal at deeper depths in the tissue. To improve reliability of this detection, the curve was smoothed with a moving averaging filter which spanned ~20μm and each detection was manually checked for reliability. In future, SPD detection can potentially be improved through use of an alternate metric which would peak at the SPD depth, such as the total vessel signal or length, however this was not explored in the context of this study. Typically, past the SPD depth, the number of independent skeleton sections fluctuate slightly due to inconsistencies in the shadowing artefact of the vasculature, until reaching the noise floor, at which point a final reduction in value is observed. The noise floor in this context is the point at which the entire *en-face* angiogram shows detected speckle-variance due to random noise in the corresponding structural images, resulting in an extremely interconnected skeleton and a low number of independent skeleton segments. Figure 4 illustrates this process for both healthy and AD skin, with healthy skin typically exhibiting a thin peak at superficial depths and AD skin typically exhibiting a much wider peak at comparatively deeper depths in the tissue.
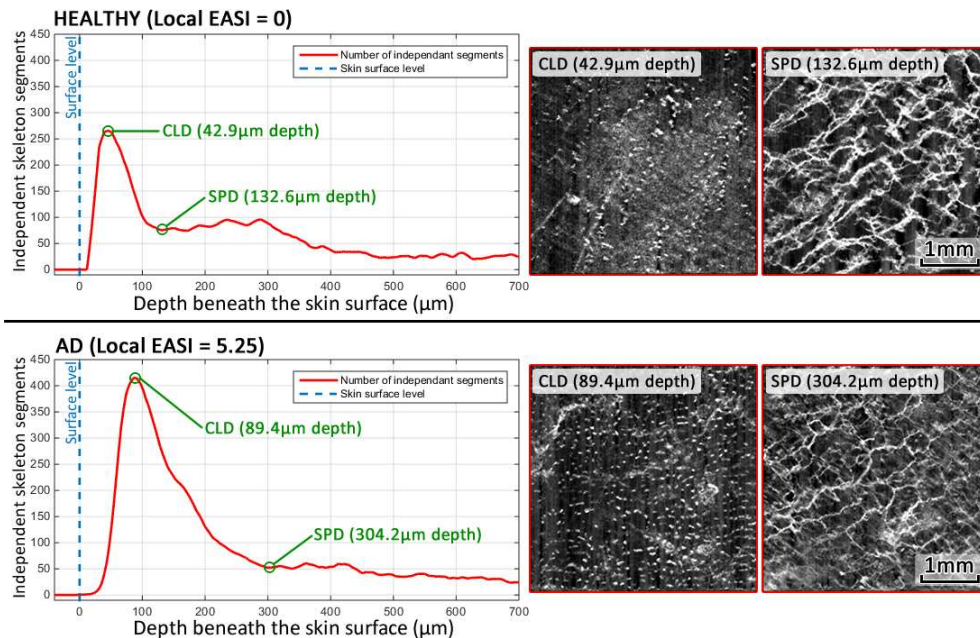
Fig. 4. Automatic measurement of CLD and SPD through consideration of the number of independent (non-connected) skeleton segments as a function of tissue depth. The top row shows the results for a healthy participant at the left cubital fossa: the local maximum (CLD) is located at 42.9μm beneath the skin surface, while the following local minima (SPD) is located at 132.6μm beneath the surface. The bottom row shows the results for a participant with AD (Local EASI = 5.25) at the left cubital fossa: the local maximum (CLD) is located at 89.4μm beneath the skin surface, while the following local minima (SPD) is located at 304.2μm beneath the surface.

2.5 Statistics

Statistical analysis was carried out using MATLAB (R2014b – Mathworks). A one-way ANOVA followed by the Tukey-Kramer honest significance difference (HSD) test was used to test for significant differences between four different data sets (Sec. 3.1). In all cases, comparisons were described as significant if the probability of the null hypothesis was <0.05. All stated and graphed measurements are of the form mean ± standard deviation.

3. Results

3.1 Scan cohorts

A total of 128 OCT data sets were acquired from the 32 participants, corresponding to 64 scans at the cubital and popliteal fossa sites respectively. To aid in analysis, these scans were separated into four different data sets based on the presence of localized AD and their local EASI score. The healthy data set (n = 20) consisted of skin sites of participants with no prior history of AD. The unaffected data set (n = 35) consisted of the skin sites of AD participants with a local EASI score of 0, thus showing no visible external symptoms of AD. The mild AD data set (n = 40) consisted of the skin sites with a local EASI greater than 0 and less than 5. Lastly the severe AD data set (n = 33) consisted of the skin sites with a local EASI greater than 5. The average global EASI score (full body) was 1.84 ± 0.92 for the unaffected data set, 4.29 ± 4.69 for the mild data set and 7.57 ± 6.62 for the severe data set. It is important to note that in this context, a skin site being allocated to the severe/mild AD data sets simply meant that the localized AD appeared severe/mild and did not necessarily imply that the global severity would be graded as severe/mild. There was however a strong correlation to this

effect, as evidenced by the comparatively higher average global EASI scores for the mild and severe AD data sets.

3.2 Automatic structural measurements of epidermal thickness

To enable comparison with the vessel derived metrics, average epidermal thickness was automatically quantified for each of the data sets using an algorithm which has been previously validated in healthy skin [15]. Briefly, this automatic algorithm first detects the air-skin (stratum corneum) boundary through application of a Sobel edge detection filter which was optimized for detecting any sharp changes in image intensity (dark to bright) in the depth-direction. Superficial detected edges which exceeded a size threshold of 15-pixels were identified and interpolated across such that the entire stratum-corneum was detected. The thresholding of smaller detected edges reduced the sensitivity of this technique to noise and other artefacts, such as superficial hairs. The second step of the automatic algorithm aimed to detect the DEJ itself, which is characterized by a transition from a hyporeflective band to a more hyperreflective band, where the grainy keratinocytes of the spinosum meet the basement membrane of the papillary dermis. This is detected as a local-minima within each A-scan [35]. Minima which are sufficiently connected are interpolated between to form the complete DEJ detection. The average distance between the detected stratum-corneum and DEJ was used as a measure of the average epidermal thickness.

To demonstrate this process, the structural OCT images seen in Fig. 5 have been averaged over 50 consecutive frames to reduce speckle-noise and improve clarity of the DEJ. The stratum corneum and DEJ in each image were segmented both manually by eye and automatically using the algorithm discussed above. Despite the averaging, the automated algorithm failed to accurately capture the complex geometry of the DEJ at the involved site, severely underestimating the true epidermal thickness. Failure in this case was determined through visual observation of each volume to check that the automatic segmentation was reasonable. This is problematic, as manual assessment of epidermal thickness is a time consuming and subjective task, particularly across volume regions of tissue. Across all data sets, detection of the DEJ using the automatic algorithm failed in 41 cases, with a high tendency towards failure at higher local EASI scores (Healthy = 1 failure, Mild AD = 11 failures, Severe AD = 29 failures). The primary reason for failure was a distinct lack of contrast at the DEJ for many of the AD skin sites. Comparatively, automatic assessment of the CLD and SPD failed in 13 cases (Healthy = 1 failure, Unaffected AD = 2 failures, Mild AD = 5 failures, Severe AD = 5 failures) with motion corrupted data being the primary reason for failure. Angiographic post-processing at the bedside would enable repeat measurements to be made in cases where motion artefacts have corrupted the data, potentially reducing the failure rates of the angiographic method. For the structural method, we believe the loss of contrast at the DEJ is related to the presence of localized acanthosis; which involves the elongation of the rete-pegs/dermal papillae into the thickening epidermis, a condition previously documented in AD affected skin [36]. The result is a highly oscillatory DEJ which rises and falls around each individual rete-peg, these sharp undulations result in the lack of a clearly defined border between the epidermis and dermis. Furthermore, it remains challenging to consistently define epidermal thickness under these conditions as measurements fluctuate between thin sections of epidermis at the tips of the dermal papillae and at comparatively thick sections of epidermis along the deepest points along each rete-peg.
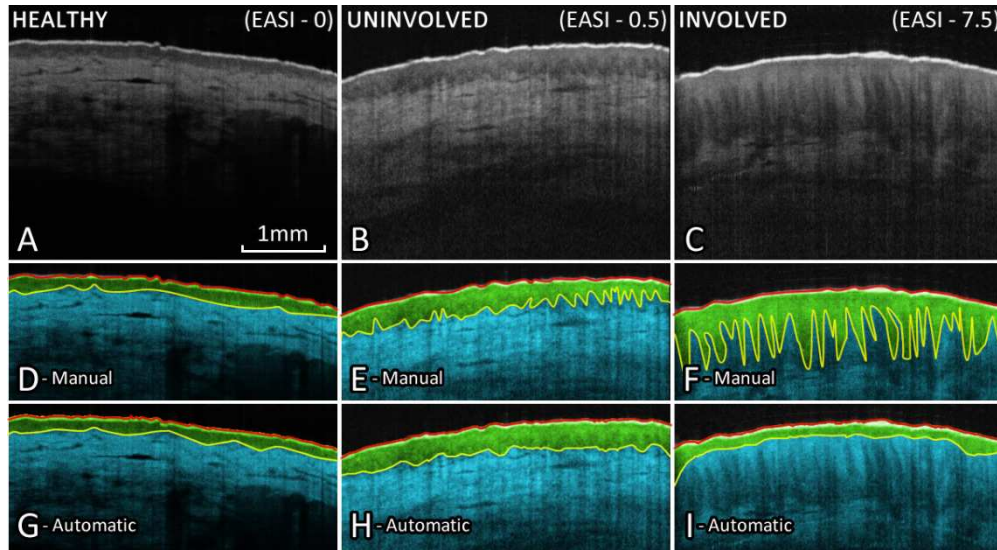
Fig. 5. Averaged (n = 50 – acquired at the same location) OCT images of the popliteal-fossa highlighting the reduction of DEJ contrast as epidermal thickness increases. A) OCT image captured from a healthy subject (Local EASI = 0), showing clear delineation of the epidermis and dermis. B) OCT image captured from an uninvolved site on an eczema patient, showing slightly extended rete-pegs and an undulating DEJ. C) OCT image captured from an involved site on a different eczema patient, showing what appears to be inflammatory acanthosis (Long thin epidermal papillae/rete-pegs). D-F) Manually segmented skin layers, for these an observer simply traced the DEJ by eye, which is laborious and potentially subjective. G-I) Automatically segmented skin layers using the algorithm described above. For D-I, red lines are the skin surface / stratum corneum layer. Green coloration represents the epidermis, Yellow-lines are the DEJ and blue coloration represents the dermis.

3.3 The effect of local severity on vascular depth

Figure 6 shows a selection of 3D angiographic data sets from each data set at each unique skin site. Each image shows the depth resolved vasculature over a depth range of 40-275μm beneath the skin surface.

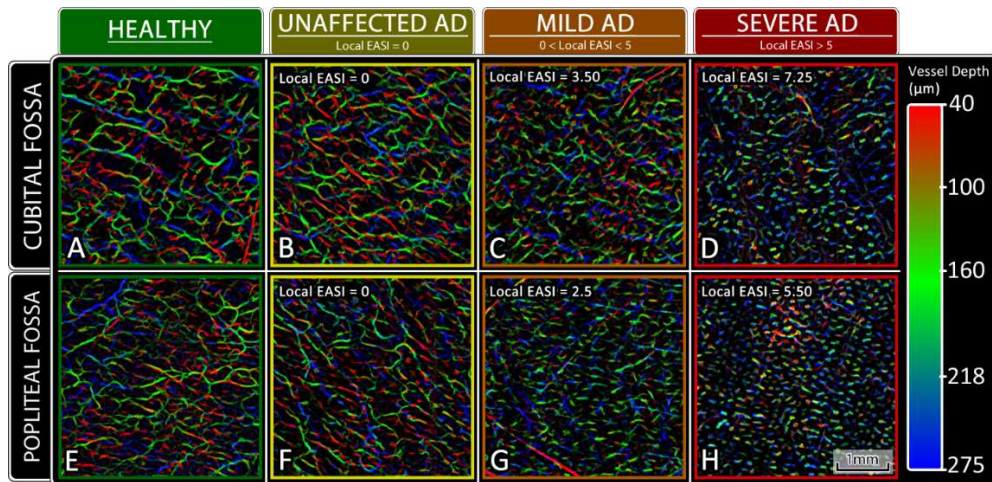Fig. 6. A selection of 3D angiographic OCT images projected over a depth range of 40-275μm beneath the skin surface. A-D) Scans from each data set captured from the cubital fossa (Elbow) skin site. E-H) Scans from each data set captured from the popliteal fossa (Knee) skin site. All images are 4x4mm.
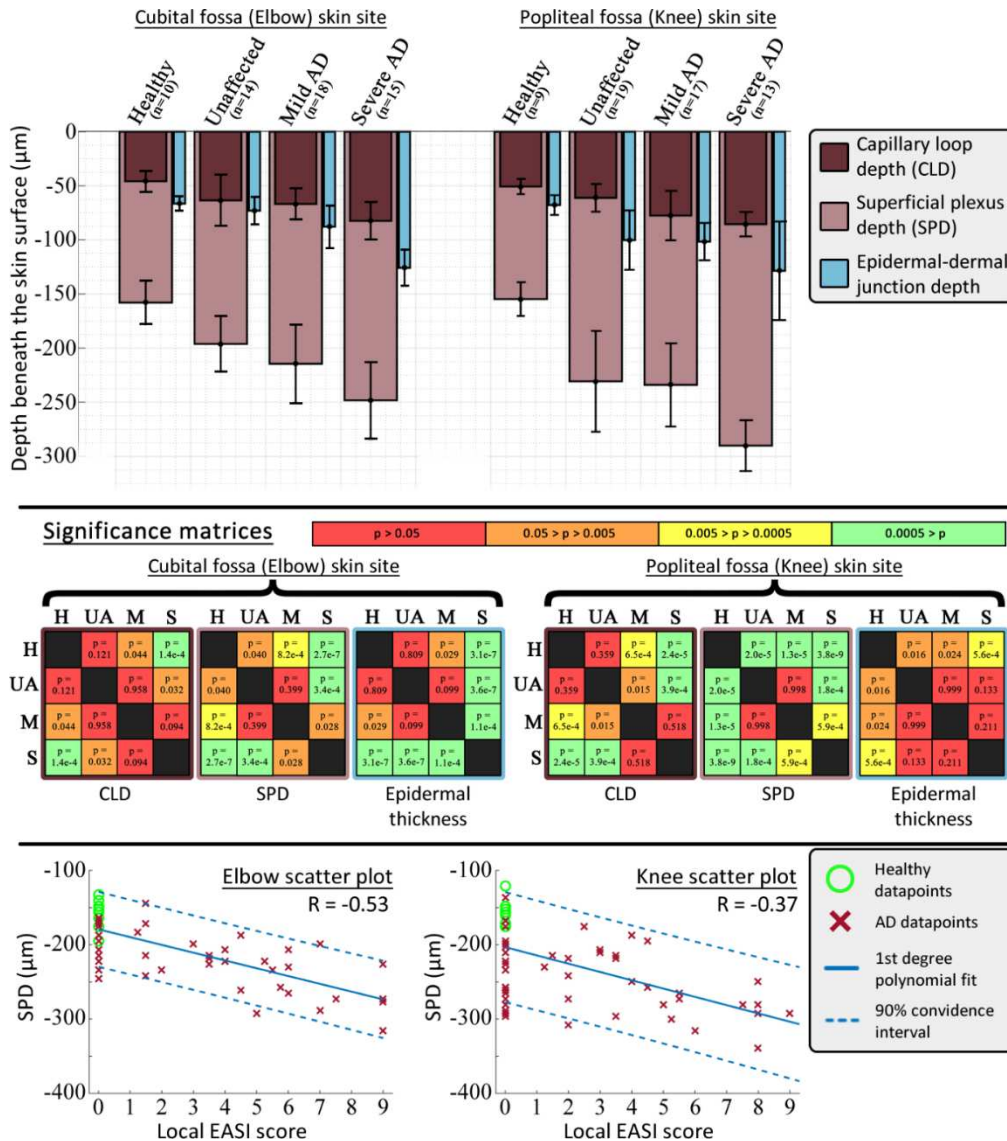
Fig. 7. Top) Charts showing differences in the CLD, SPD and epidermal-dermal junction depth at both the cubital fossa and popliteal fossa skin sites for a range of AD severities. Columns: Mean depth. Bars: Standard deviation. Significance was calculated at each skin site independently using a one-way ANOVA followed by the Tukey-Kramer honest significance difference (HSD) test. Significance matrix colors correspond to the measured p-value (p>0.05 - Red, 0.05>p>0.005 - Orange, 0.005>p>0.0005 - Yellow, 0.0005>p - Green). Quoted data set sizes reflect angiography measurements only, as automatic epidermal-dermal junction assessment failed in a greater number of cases (With a bias towards failing in severe AD cases). Cohort sizes for the epidermal-dermal junction values were as follows: (From left to right): n = 9, 12, 14, 7, 9, 18, 13, 5. Bottom) Scatter plots showing the ungrouped SPD as a function of local EASI score, with a negative correlation visible at both sites. 1st degree polynomial fit was generated using all data points (Including healthy data).

For the healthy data sets seen in Fig. 6, a highly connected plexus was visible over this depth range, suggesting that the epidermis remains relatively thin. In contrast, in cases of severe localized AD, numerous dots (capillary loops) could be seen with very few connecting vessels joining them together. As expected, this suggests that a thickened epidermis is present, as the superficial plexus has been pushed deeper into the tissue (>275μm). Cases of

unaffected or mild localized AD appear to bridge this gap with the connecting vascular plexus becoming less visible as the epidermis thickens.

Figure 7 summarizes the results of automatic quantification of the CLD, SPD and epidermal-dermal junction depth across the entire data set. Measurements of the epidermal thickness (Blue columns) were included for comparative purposes. As expected due to localized inflammation, the thickness of the epidermis increases as the severity of localized AD increases. However, particularly for mild or severe cases of localized AD, the reported value of mean epidermal thickness is likely to be underestimated. This is a result of the automatic epidermal-dermal junction segmentation algorithm having an increased tendency to fail at thicker skin sites compared to areas with a thinner epidermis as discussed in Sec. 3.2 as evidenced by the comparatively smaller cohort sizes used for the mild/severe AD epidermal thickness measurements. This may explain the lack of any significance differences between the epidermal thickness of unaffected, mild and severe localized AD at the popliteal fossa skin site, as any thicknesses above approximately 100μm are unlikely to be measured accurately.

Both the CLD (purple columns) and SPD (red columns) follow a similar trend to that of epidermal thickness, with an increase in depth as the severity of the localized AD increases (Fig. 7). For the case of the CLD, the differences are relatively small, with no significant differences found between the healthy and unaffected data sets at either skin site. Significant differences in CLD depth were however found between the healthy data set and the mild/severe data sets at both skin sites, suggesting that a significantly deepened CLD may be an indicator that the condition is clinically active with moderate localized severity. The SPD displayed comparatively greater differences between each data set. Of particular interest, significant differences in SPD were found between the healthy and unaffected data sets at both the elbow ($p = 0.04$) and the knee ($p<0.001$), suggesting that this metric could be used to as a means of differentiating between the two. This could prove useful when aiming to monitor the efficacy of a treatment for AD, past the point of clinical remission. Furthermore, for both skin sites, significant differences in SPD were recordable between the healthy and mild/severe data sets as well as between the severe and unaffected/mild data sets. This suggests that the metric may remain robust and be able to differentiate between more severe cases of the condition.

Of potentially greater interest, SPD depth did discriminate between healthy (do not suffer from AD) skin and skin at the site of a healed flare (i.e. "unaffected"), whereas EASI did not (both skin types are assessed as EASI = zero). Similarly, no OCT-derived parameter, structural or angiographic, provided a strong discrimination between skin scored as unaffected and skin scored as mildly inflamed, even though the EASI scores are different. This could indicate that what is clinically scored as "healed" skin retains some physically detectable traits which are characteristic of mildly inflamed skin. In general, all three metrics followed a negative correlation as the local AD severity increased, suggesting that vascular measurements of CLD and SPD may have potential as robust measures of skin inflammation alongside epidermal thickness. Such measurement of the vascular layers may prove useful for monitoring the delicate balance between epidermal atrophy and acanthosis in response to topical corticosteroid application [17,19,37], particularly in areas of extreme thickening. Furthermore, since the inflammatory skin of AD can be characterized by altered angiogenesis [38,39], the depth and shape of the vasculature may hold additional information regarding the state of inflammation that is not provided by simple measures of epidermal thickness. Future research may focus on monitoring baseline variations of these parameters within the same patient over a period of time, a case where biological variability is far less likely to influence the data.

The scatter plots shown at the bottom of Fig. 7 show how the ungrouped SPD measurements vary as a function of the local EASI score. While there is a negative correlation visible between the SPD depth and local EASI score at both the elbow ($R = −0.53$) and knee

(R = −0.37), the variation in the recorded measurements is high. This makes it unlikely that accurate estimates of the local EASI score could be inversely attained from measurements of the SPD depth. In a sense this is not concerning, as 100% correlation would imply that the SPD biomarker, which is technically difficult and expensive to measure, offers no additional information over EASI score, which is cheap and easy to assess by eye. Given that much of this variability can also likely be attributed to biological variations in the skin between different volunteers, one potential avenue of future work will be assessing how much variation remains when considering intra-patient measurements over a period of time. Furthermore, local EASI is a composite metric, combining multiple skin features (redness, excoriation, oedema and lichenification) in order to quantify the severity of the condition. The current study population was deemed insufficient for stratification on the individual signs, but it may be that SPD correlates more robustly with a particular sign. This idea is to be assessed in the future.

3.4 The effect of severity on vascular morphology in the superficial vascular plexus

One key output of the angiographic OCT processing technique is the availability of depth-resolved *en-face* visualizations of the vascular network. The skin of patients with AD can be characterized by an abnormal erythematous vascular pattern visible from the surface of the skin [40]. Furthermore it is known that such patients exhibit abnormal vasoconstrictive responses to stimuli, including mechanical pressure (white dermographism [25]) and temperature [24]. Previously, differences in the microcirculatory flow of AD patients following treatment with a pimecrolimus cream have been quantified using laser doppler flowmetry [41]. Furthermore svOCT has been utilized to demonstrate the relevance of morphological vascular changes within inflammatory skin conditions including psoriasis and scleroderma [22]. Combined angiographic OCT and photoacoustic imaging has previously detected abnormal morphology and even potential micro aneurisms within skin affected by AD [42]. Thus, it is highly likely that the morphology of the vessels themselves will present some information regarding the severity of the AD.

Previously we have shown that measurable morphological differences between healthy and AD scans are attainable using svOCT depth projections over a wide depth range (30-300μm) [32], however it is unclear if the differences were related to true morphological differences or simply a result of the AD vessels being much deeper in the skin. To investigate this, the SPD data from Sec. 3.3 was utilized to acquire depth projections only over the depth range of the SPD (± 30μm). For example, if the SPD was recorded at a depth of 200μm, a projection image for quantification would be generated over the range 170-230μm, normalizing the depth considered to that of the SPD. This projection image was then skeletonized and quantified following the methodology outlined in Sec 2.3.

Figure 8 shows a selection of the depth projected angiographic images which were used for quantification, while Fig. 9 shows the results of the quantification. Due to the sensitivity of these measurements to noise, and as discussed in Sec. 2.2, only scans which were acquired using the higher quality scan settings (10μm y-resolution) and which were deemed sufficiently noise free were used for these measurements, resulting in a reduction in overall group size. Qualitative observation of the angiographic SPD images shown in Fig. 8 shows the morphology of scans in the healthy, unaffected AD and mild AD cohorts are difficult to differentiate, as they all display long, thin vascular morphology. Comparatively scans of sites with severe localized AD showed a dense network of small, comparatively wide vessels.
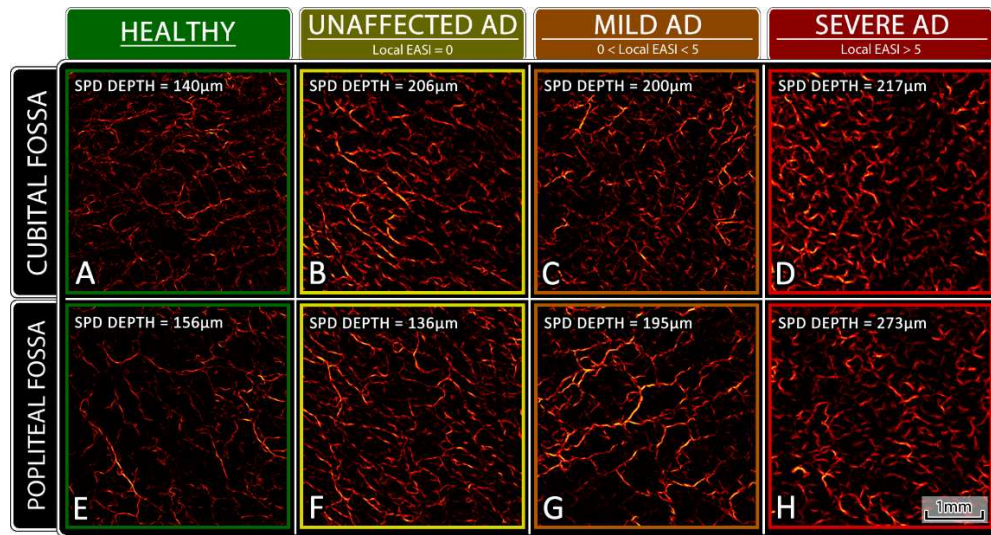
Fig. 8. A selection of 2D angiographic OCT images projected over a depth range of ± 30μm around the detected SPD depth, showing morphological differences in the SPD. A-D) Scans from each data set captured from the cubital fossa (Elbow) skin site. E-H) Scans from each data set captured from the popliteal fossa (Knee) skin site. All images are 4x4mm.

Through the quantitative measurements shown in Fig. 9, the measured mean vessel diameter was found to be significantly higher for patients with severe localized AD, when compared to all other data sets at both skin sites. The sole exception being the unaffected elbow, which did not quite reach significance ($p = 0.058$). Vascular enlargement is one of the primary alterations to the cutaneous circulation within inflammatory skin conditions such as AD, psoriasis and rosacea [43], thus it is unsurprising that the vessel diameter is measurable larger for severe cases of localized AD.

Mean vessel segment length was significantly higher in the healthy data set than in the severe AD data set at both skin sites. This suggests that for severe localized AD patients, the individual vessel segments are shortened, with more branch points. There was however no significant discrimination in vessel segment length between healthy skin and skin graded as unaffected or mildly inflamed. Vessel density was found to be significantly higher for the severe AD data set when compared to all other data sets, with the unaffected elbow being the exception ($p = 0.108$). In general, these two metrics correspond to an observed increase in vessel growth and branching within the severe AD data set. This is expected, as lesioned skin affected by AD has previously been shown to exhibit higher levels of the angiogenic growth factor VEGF compared to healthy skin [44,45], which is associated with increased levels of vascular remodeling [46].

Lastly, the differences in fractal dimension between the healthy and severe data sets did not reach significance at the elbow site ($p = 0.098$), however a significant increase in fractal dimension was found for higher severities at the knee site suggesting those vessel networks became more tortuous and irregular as severity increased. Previously, the study of the fractal dimension of vascular networks has proven to be a fast, reliable and robust parameter for observing and evaluating angiographic processes [47], thus it may prove a useful metric when considering the increased angiogenic proliferation within AD.
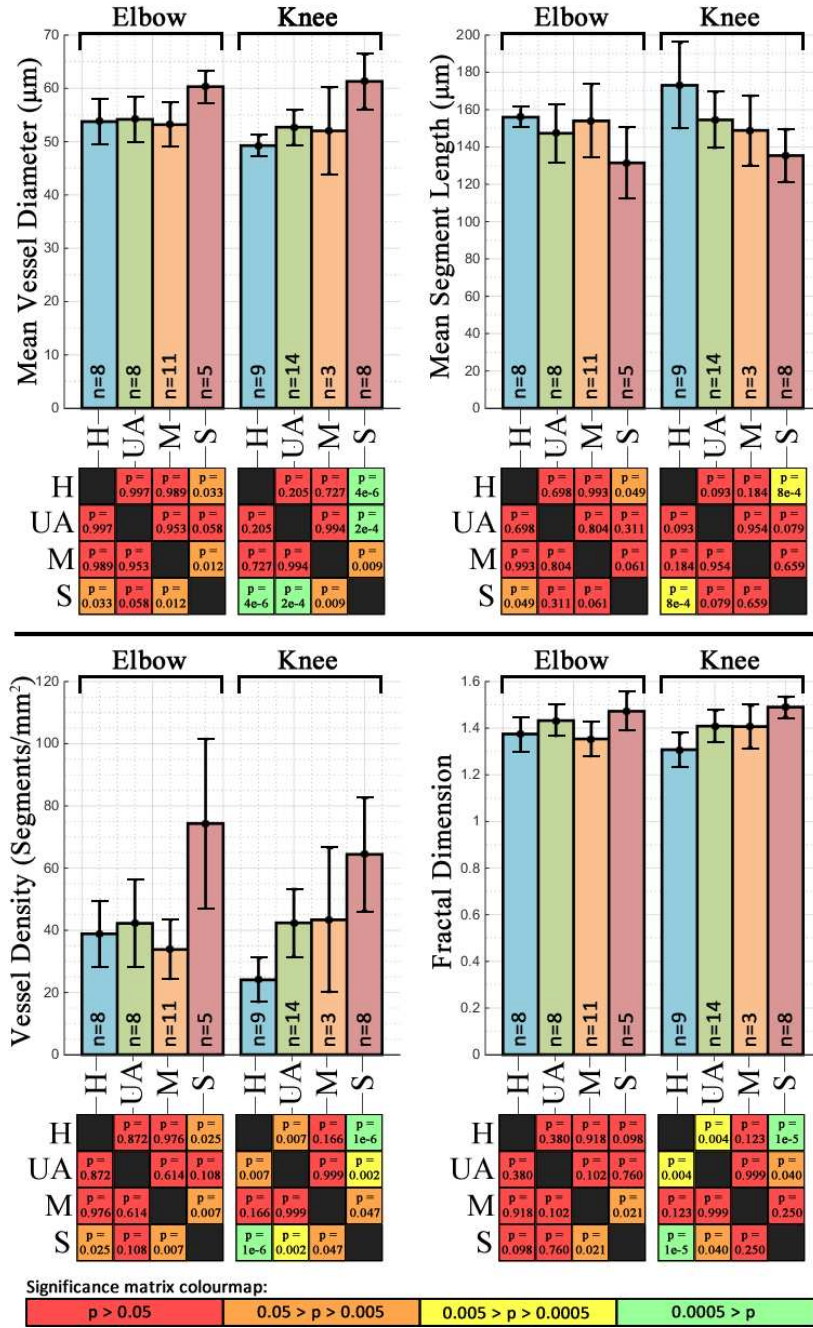
Fig. 9. Bar charts showing the variance of quantitative parameters which were automatically extracted from the superficial vascular plexus layer of data sets following the binarization and skeletonization steps outlined in section 2.3. Columns: Mean depth. Bars: Standard deviation. Significance was calculated at each skin site independently using a one-way ANOVA followed by the Tukey-Kramer honest significance difference (HSD) test. H = Healthy, U = Unaffected, M = Mild localized AD, S = Severe localized AD. Numbers at the base of each column correspond to group size (n).

4. Conclusions

Unequivocal assessment of the severity of AD is a challenging and subjective task to perform, particularly within flare-free AD patients. This is a result of many of the external, clinical features of the condition being characteristic, but not specific indicators of severity. Sub-clinical measurements of epidermal thickening remain robust for areas exhibiting mild symptoms, but become increasingly difficult as the epidermis increasingly thickens due to the extension of the dermal papillae during acanthosis. Here we demonstrate how the visualization and quantification of the microcirculatory depth using OCT can be utilized as an alternative means of achieving this measurement, as the superficial plexus remains relatively flat regardless of its depth within the tissue. It is shown that the superficial plexus depth (SPD) differs significantly between healthy patients and those who are unaffected or suffering from mild or severe localized AD, and thus can potentially be utilized as a metric for monitoring the severity of the condition. Recent treatment strategies for AD emphasize the importance of treating a flare (e.g. with topical corticosteroids) beyond the point at which visible lesions have disappeared. Of particular relevance to this idea, we have shown that the SPD metric differs significantly (p = 0.04 at the elbow, p = 2.0×10^{-5} at the knee) between healthy (do not suffer from AD) subjects and AD subjects whose flares have indeed disappeared visually. Hence SPD depth has potential as a non-invasive biomarker of sub-clinical inflammation. Furthermore, the morphology of the vessels themselves appear to be altered with the presence of AD, with significant changes in vessel diameter, length, density and fractal dimension between healthy and severe localized AD patients. These metrics provide a means of quantifying and differentiating between subtle changes in the condition, particularly past the point of clinical-remission.

Limitations of the current study include the need to make physical contact with the skin surface, which may induce some degree of vasoconstriction within the observed vessels. Contactless scans were deemed impractical at the imaging speeds used herein, but faster OCT systems could potentially be used to acquire contactless angiographic scans without inducing excessive motion artefacts in the data. Furthermore, we only considered one algorithm for measuring the structural epidermal thickness. It is possible that more advanced detection algorithms will have a greater success rate for DEJ detection and should be considered moving forward.

Future developments will focus on the further refinement of both angiographic and structural detection methods. In particular, the application of the techniques described herein to long-term clinical observations of drug and treatment efficacy may help to assess clinical benefit. Angiographic OCT may also provide a valuable guide to determining how long treatments for AD should be continued after visible lesions have resolved, in order to induce clearance of all sub-clinical manifestations of AD. This OCT biomarker can therefore be used to stratify patients into those requiring different durations of therapy to achieve optimal long-term control of their AD. Angiographic OCT could also be used to determine the long-term safety of therapies such as topical corticosteroids, by providing a robust, non-invasive measure of epidermal atrophy.

Disclosures

The authors declare that there are no conflicts of interest related to this article.